Analysis of Peak Ground Acceleration and Seismogenic Fault Characteristics of the Mw7.8 Earthquake in Turkey

Yushi Duan *, Jingshan Bo, Da Peng, Qi Li, Wei Wan, Wenhao Qi

Posted Date: 5 September 2023

doi: 10.20944/preprints202309.0237.v1

Keywords: Turkey earthquake; peak ground acceleration; seismogenic fault; near-fault effect; fault locking segment effect; trampoline effect

Article

Analysis of Peak Ground Acceleration and Seismogenic Fault Characteristics of the Mw7.8 Earthquake in Turkey

Yushi Duan [1,2], Jingshan Bo [1,2]*, Peng Da [1], Qi Li [1], Wei Wan [1,2]and Wenhao Qi [1]

[1] Key Laboratory of Earthquake Engineering and Engineering Vibration, Institute of Engineering Mechanics, China Earthquake Administration, Harbin 150080, China;
[2] Institute of Disaster Prevention,Sanhe 065201,China.
* Correspondence: duanyushi2023@163.com

Featured Application: This paper investigates the peak ground acceleration (PGA) and seismogenic fault characteristics of the Mw7.8 earthquake that struck Turkey on February 6, 2023. The paper identifies the near-fault effect, the fault locking segment effect and the trampoline effect of the earthquake, and presents a detailed spatial distribution of PGA. The featured application of this work is in seismic engineering and disaster prevention, where the PGA and fault characteristics are essential for assessing the seismic demand and capacity of structures, as well as the potential damage and loss induced by earthquakes. The paper also enhances the understanding of the seismogenic mechanism, damage mode, characteristics and strong earthquake law of Turkey earthquake, which can facilitate the improvement of the seismic design codes and emergency response plans in Turkey and other regions with similar tectonic settings.

Abstract: A Mw7.8 earthquake struck Turkey on February 6, 2023, causing severe casualties and economic losses. This paper investigates the characteristics of strong ground motion and seismogenic fault of the earthquake. We collected and processed the strong ground motion records of 379 stations using Matlab, SeismoSignal and Surfer software, and obtained the peak ground acceleration (PGA) contour map. We analyzed the near-fault effect, the fault locking segment effect and the trampoline effect of the earthquake based on the spatial distribution of PGA, the fault geometry and slip distribution. We found that the earthquake generated a very strong ground motion concentration effect in the near-fault area, with the maximum PGA exceeding 2000cm/s^2. However, the presence of fault locking segments influenced the spatial distribution of ground motion, resulting in four significant PGA high-value concentration areas at a local dislocation, a turning point and the end of the East Anatolian Fault. We also revealed for the first time the typical manifestation of the trampoline effect in this earthquake, which was characterized by a large vertical acceleration with the positive direction significantly larger than the negative direction. This paper provides an important reference for understanding the seismogenic mechanism, damage mode, characteristics and strong earthquake law of Turkey earthquake.

Keywords: Turkey earthquake; peak ground acceleration; seismogenic fault; near-fault effect; fault locking segment effect; trampoline effect

1. Introduction

The The term "strong motion" refers to the intense shaking experienced during an earthquake. It is a measure of the ground acceleration, velocity, and Observation entails the documentation of acceleration time-history curves of ground motion occurring during earthquakes, with the purpose of studying the ground motion phenomenon and the reaction of engineering structures. The exploration of this subject matter has emerged as a pivotal field of study within contemporary seismology and earthquake engineering.

 doi:10.20944/preprints202309.0237.v1

The Anatolian Peninsula is recognized as a highly dynamic seismotectonic area, characterized by a significant occurrence of destructive earthquakes throughout the last century. To monitor such events, Turkey has deployed a substantial number of strong motion accelerographs since 1973 [1]. At present, there are a total of 762 operational strong motion stations that are actively producing approximately 20,000 strong motion records on an annual basis [2,3]. These records provide crucial data for earthquake disaster defense and emergency response. Scholars from various countries have conducted extensive research based on Turkey's seismic network and strong motion records: In their study, Akkar et al. [4] conducted an analysis of earthquake spectral characteristics, attenuation laws, and near-field effects. Their research aimed to gain a deeper understanding of the physical mechanisms behind ground motion and to enhance seismic hazard assessment; Beyhan et al. [5] examined the correlation between strong motion records and various categories of structural seismic performance, damage patterns, and vulnerability curves. Their research aimed to gather data and insights that could be used to evaluate structural seismic damage and develop seismic design guidelines. Bommer et al. [6] established a shallow crustal ground motion prediction model, offering a reliable tool and parameters for nonlinear dynamic analysis.

Nevertheless, certain limitations persist in the present research. Strong motion data can be subject to various issues that can impact its quality and reliability. These issues include instrument errors, baseline drift, and digitization distortion. On the other hand, in terms of research direction, there is still a lack of studies that combine strong motion records with the relationship to seismogenic faults. Additionally, a comprehensive analysis of the influence of various fault types, locations, and geometric configurations on strong ground motion is currently lacking.

The objective of this study was to gather and systematically arrange strong motion records obtained from the Mw7.8 earthquake that took place in Turkey on February 6, 2023. The spatial distribution patterns and characteristics of strong ground motion in this earthquake were analyzed. This report provides a summary of the correlation between ground motion and the resulting seismic damage. Additionally, it explores the association between strong motion records and seismogenic faults. Preliminary analyses were conducted concerning near-fault effects, locked segment effects, and trampoline effects based on the geometric features of seismogenic faults. The research presented offers essential insights into the seismogenic mechanism, damage patterns, and characteristics of the earthquake under investigation. Additionally, it functions as a fundamental framework for conducting comprehensive investigations on seismic characteristics and strong motion patterns in Turkey.

2. Regional Tectonics and Earthquake Overview

Turkey is located at the junction of Eurasia, on the Anatolian Plate, which is affected by the interaction of several adjacent plates and fault zones[7], as shown in Figure 1: a. The Arabian Plate squeezes the Anatolian Plate to the northwest, forming the East Anatolian Fault Zone that is the most active fault zone in Turkey in recent years; b. The African Plate, located south of Turkey, subducts northward under the Eurasian Plate, forming the Greek Island Arc, which is the most active subduction zone in Europe; c. The Eurasian Plate, located north of Turkey, squeezes Turkey's northern part southward, forming the North Anatolian Fault Zone, which is a right-lateral strike-slip fault zone extending from the northwest of Turkey to the east of Georgia, and also the longest fault zone in Turkey[8–10].

The specific time of this earthquake was 01:17 on February 6, 2023, and the seismogenic fault was the East Anatolian Fault Zone[11]. The fault zone stretches about 700 kilometers from the eastern to the central-southern part of Turkey, forming a deformation-type tectonic boundary between the Anatolian Plate and the northward-moving Arabian Plate. The slip rate in the east is 6-10mm/year, and in the west is 1-4mm/year[12]. The fault can also be divided into different directions of secondary faults, with mostly left-lateral slip, and locally showing thrust or normal faults[13].

Preprints (www.preprints.org) | NOT PEER-REVIEWED | Posted: 5 September 2023 doi:10.20944/preprints202309.0237.v1

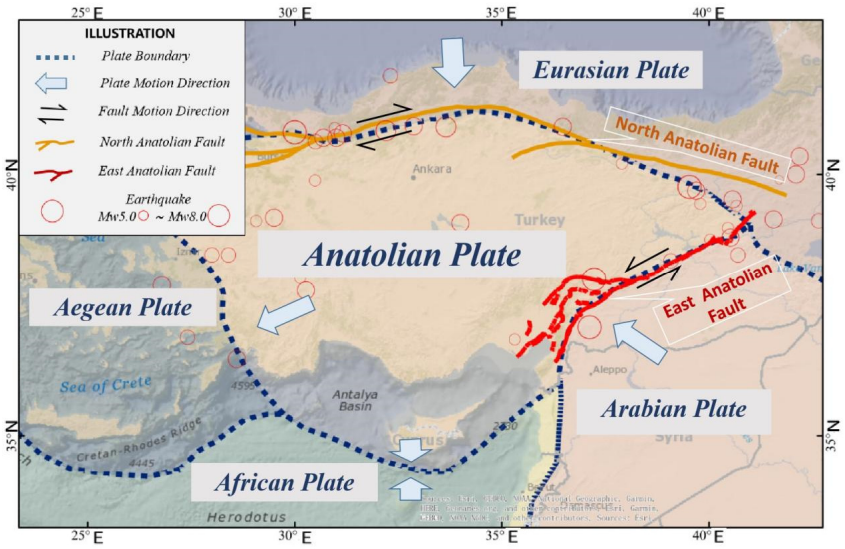

Figure 1. Schematic diagram of the relevant plates and active faults around Turkey.

The epicenter was located in Pazarcık district of Kahramanmaraş city in Gaziantep province of Turkey, with a focal depth of 10km. This earthquake caused extremely severe disasters in southern Turkey and northern Syria, and was the strongest earthquake in the region in more than a hundred years[14]. (See Table 1 for details of the earthquake)

Table 1. Statistical table of the earthquake basic information.

Basic Facts	Date&Time	February 6,2023,01:17（UTC）
	Location	Pazarcık
	Latitude(°)	37.288
	Longitude(°)	37.043
	earthquake magnitude	Mw7.8
Seismogenic Structure	hypocentral depth(km)	10
	Fault	East Anatolian Fault
	Rupture Length(km)	70
Peak Value	PGA(cm/s²)	2039.20
	PGV(cm/s)	186.78
	PGD(cm)	142.08
Damage Loss	direct physical damages(dollars)	34.2 Billion
	Casualty	59259

The earthquake caused a direct economic loss of 34.2 billion US dollars[15] in Turkey, and resulted in large-scale casualties and building damage. There were 59,259 people killed in the earthquake, which was the most deadly one in Turkey since 1900[15]. Among them, Gaziantep city was the most severely affected city, with more than 15,000 people dead and more than 30,000 injured. The Şehitkamil district, which was closest to the epicenter, had 12,141 buildings destroyed or severely damaged, with a building damage rate of more than 80%[14]. The Gaziantep Castle was the oldest building damaged in the earthquake, with a history of more than two thousand years, and had extremely precious cultural value[16]. Figure 2 shows the comparison of the castle before and after the earthquake. The earthquake also caused serious disasters in Hatay, Kahramanmaraş, Malatya, Adıyaman, Diyarbakır, Şanlıurfa, Mardin and other cities and regions. These seismic damages included building collapse (see Figure 3), surface rupture (see Figure 4), landslide (see Figure 5), sand soil liquefaction (see Figure 6) and so on[17–19].

Preprints (www.preprints.org) | NOT PEER-REVIEWED | Posted: 5 September 2023 doi:10.20944/preprints202309.0237.v1

Figure 2. Comparison of Gaziantep Castle before and after the earthquake.

Figure 3. Comparison of Trend Garden Residence Hotel before and after the earthquake

Figure 4. Comparison of surface rupture before and after the earthquake

Figure 5. Comparison of landslide before and after the earthquake

Figure 6. Comparison of site liquefaction before and after the earthquake

3. Materials and Methods

3.1. Data Sources

The strong motion data utilized in this study were acquired from Turkey's Disaster and Emergency Management Authority (AFAD). Following the occurrence of the earthquake, the

Preprints (www.preprints.org) | NOT PEER-REVIEWED | Posted: 5 September 2023 doi:10.20944/preprints202309.0237.v1

aforementioned agency promptly disseminated pertinent strong motion record data on its official website. Subsequently, the data underwent several calibrations and updates [20]. The data used in this study are from the version published on June 1, 2023, comprising records from 379 stations. The distribution of peak ground acceleration (PGA) and station locations is shown in Figure 7. The strong motion instruments and sensor models for each station are listed below: There are a total of 87 stations that are equipped with the GEOSIG GMS AC-73 seismic instrument. Additionally, there are 140 stations that utilize the Uralp CMG-5T instrument. Furthermore, there are 107 stations that make use of the SARA ACEBOX sa10 instrument. Lastly, there are 45 stations that employ various other seismic instruments [21]. Table 2 presents a compilation of strong motion records acquired from the earthquake under consideration. The table includes relevant details such as station numbers, latitude and longitude coordinates, peak ground acceleration (PGA) values, epicentral distances, fault distances, and station locations. This information has been included in the table due to spatial constraints.

3.2. Strong Motion Record Screening and Processing

During the initial screening of the raw data, the study observed a phenomenon in which a small number of station records displayed 'truncated' characteristics. For instance, at Station 0208 (as shown in Table 2), despite being only 1.67 km away from the fault, the recorded PGA was only around 30 cm/s² (significantly lower than the average acceleration within 5 km of the fault, which exceeds 500 cm/s²). The record had a duration of fewer than 8 seconds. Station 0214 demonstrated analogous behavior, as it was located at a distance of 2.91 km from the fault and experienced a peak acceleration below 70 cm/s2. Nineteen stations in the acquired strong-motion records displayed the previously mentioned 'truncated' characteristics. Further analysis revealed that most of these stations were located closer to the fault or epicenter. Additionally, it should be noted that station 4702 exhibited a deficiency in its seismic motion records. Specifically, this station only captured seismic motion along the east-west and vertical axes, while lacking data for the north-south direction. The recorded magnitudes were approximately 15 cm/s² for the east-west and vertical directions, whereas the north-south direction only registered a magnitude of 0.4 cm/s². To ensure data accuracy, this study excluded the aforementioned 20 records that potentially had anomalous data. The acceleration data was subjected to batch processing using Matlab software. Subsequently, the records that required additional analysis were further processed using the SeismoSignal software. This involved performing baseline correction and applying Butterworth high-pass filtering.

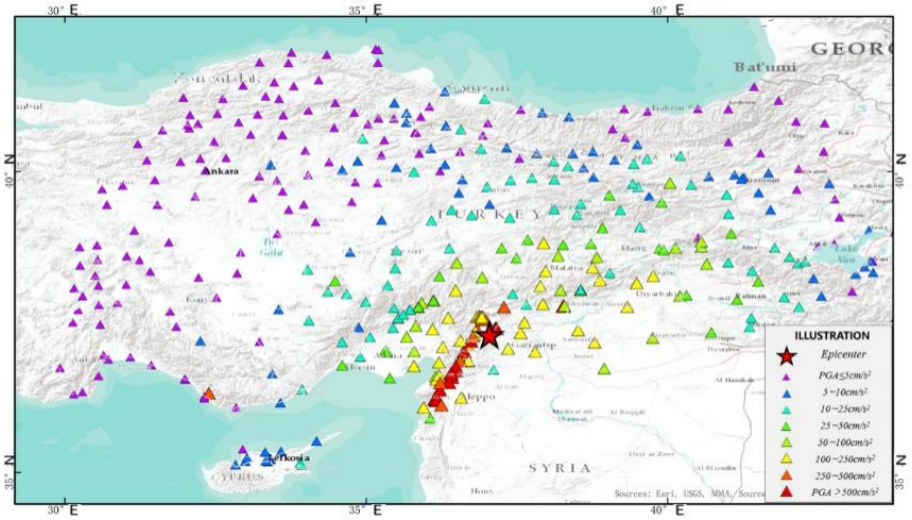

Figure 7. Distribution of seismic recording stations and PGA.

Preprints (www.preprints.org) | NOT PEER-REVIEWED | Posted: 5 September 2023 doi:10.20944/preprints202309.0237.v1

3.3. Preliminary Analysis of the Characteristics of PGA Distribution

According to Table 2, the earthquake's highest Peak Ground Acceleration (PGA) values were recorded at station 4614, which is situated in Kahramanmaraş City. Its PGA values in all three directions were the largest among all stations (north-south: 2039.20 cm/s², east-west: 2016.99 cm/s², vertical: 1582.62 cm/s²). Figure 8 displays the PGA time-history curve pertaining to station 4614. The PGA value of 1372.07 cm/s², which ranks as the second-largest in the east-west direction, was documented at station 3135 in Arsuz. This measurement was obtained at a fault distance of 33.44 km. The second-largest north-south PGA value (1351.50 cm/s²) was recorded at station 3129 in Defne, with a fault distance of 2.42 km. The second-largest vertical PGA value (1151.56 cm/s²) was recorded at station 3129 in Hatay, with a fault distance of 5.15 km.

Table 2. Compilation table of seismic recording data.

Station	District	Lon.	Lat.	Repi.（km）	Rrup.（km）	PGA_E（cm/s²）	PGA_N（cm/s²）	PGA_U（cm/s²）
0208	Gölbaşı	37.653	37.787	77.255	1.67	14.00	30.20	16.97
0214	Çelikhan	38.226	38.028	132.738	2.91	54.38	61.68	69.91
2712	Nurdağı	36.732	37.184	29.85	1.10	592.35	555.59	313.75
2718	İslahiye	36.627	37.008	48.33	1.45	630.31	654.43	592.28
3123	Hatay	36.160	36.214	142.92	1.72	593.94	655.57	867.58
3125	Hatay	36.133	36.238	142.09	5.15	1121.95	822.62	1151.56
3129	Defne	36.134	36.191	146.39	2.42	1198.74	1351.50	716.94
3134	Dörtyol	36.205	36.828	90.39	28.95	203.91	246.11	141.51
3135	Arsuz	35.883	36.409	142.23	33.44	1372.07	740.97	588.97
3137	Hatay	36.489	36.693	82.46	0.39	670.17	428.37	448.37
4614	Kahramanmaraş	37.298	37.485	31.42	6.81	2039.20	2016.99	1582.62
4615	Kahramanmaraş	37.138	37.387	13.82	11.28	556.65	584.65	656.68
4626	Onikişubat	36.915	37.575	33.84	16.15	223.09	108.81	112.27
4702	Midyat	41.357	37.417	381.59	248.63	21.33	0.38	15.82
7901	Kilis	37.112	36.709	64.57	50.92	16.55	53.11	50.14
8002	Osmaniye	36.562	37.192	44.01	14.19	202.89	242.95	336.56
8004	Kadirli	36.100	37.380	181.86	168.43	181.86	168.42	71.780

Furthermore, it has been observed that certain north-south peak ground acceleration (PGA) values exhibited a notable disparity when compared to the east-west PGA values in the context of this earthquake. Station 7901, situated in Kilis, exhibited a north-south peak acceleration of 53.11 cm/s², which is 3.2 times greater than the east-west peak acceleration of 16.55 cm/s². Similarly, for some stations, the east-west peak acceleration was notably larger than the north-south component. For instance, station 4626 in Onikişubat had an east-west peak acceleration of 223.09 cm/s², which is 2.05 times that of the north-south peak acceleration (108.81 cm/s²). nstances were observed where the vertical peak acceleration surpassed the magnitude of acceleration in the horizontal direction. An example of this can be seen at station 3123 in Hatay, where the vertical peak acceleration measured was 867.58 cm/s². This value is 1.46 times higher than the east-west peak acceleration recorded at 593.94 cm/s².

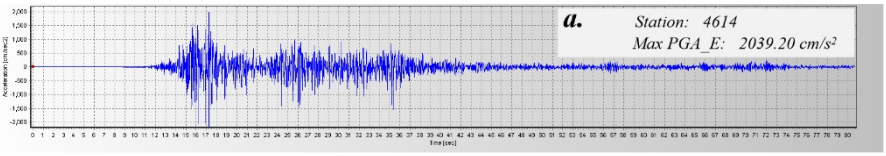

Preprints (www.preprints.org) | NOT PEER-REVIEWED | Posted: 5 September 2023 doi:10.20944/preprints202309.0237.v1

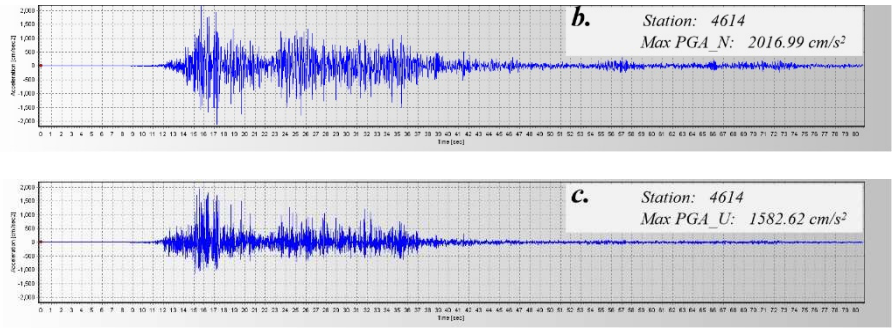

Figure 8. PGA time-history curve for station 4614.

The recorded data comprises information gathered from multiple stations, with a specific focus on strategically positioning some of these stations near the East Anatolian Fault. The nearest station to the fault is station 3139, located at a distance of only 0.06 kilometers. There are additional stations in close proximity to station 3137, such as station 3123 which is located 1.72 km away. There are a total of 22 stations located within a 10-kilometer radius of the fault, while 49 stations are situated within a 50-kilometer radius. The acquisition of near-fault seismic records is of utmost importance in order to gain a comprehensive understanding of near-field seismic characteristics. These records play a vital role in establishing precise attenuation relationships and revealing the scale and faulting characteristics of seismic faults [22,23].

Using Surfer software and employing Kriging interpolation, this study generated contour maps of PGA values for three directions based on the collected strong motion data. depicts the spatial distribution of Peak Ground Acceleration (PGA) values observed in the earthquake event. Subsequent sections will conduct a more detailed analysis and discussion of the seismic effects, building upon the examination of Figure 9.

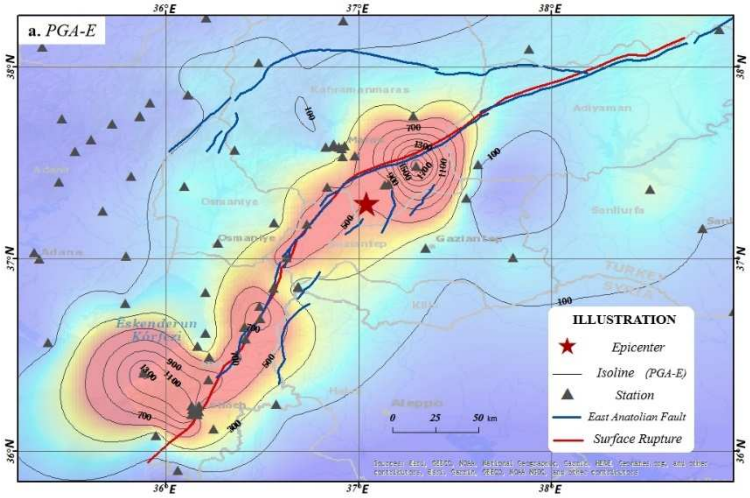

Preprints (www.preprints.org) | NOT PEER-REVIEWED | Posted: 5 September 2023 doi:10.20944/preprints202309.0237.v1

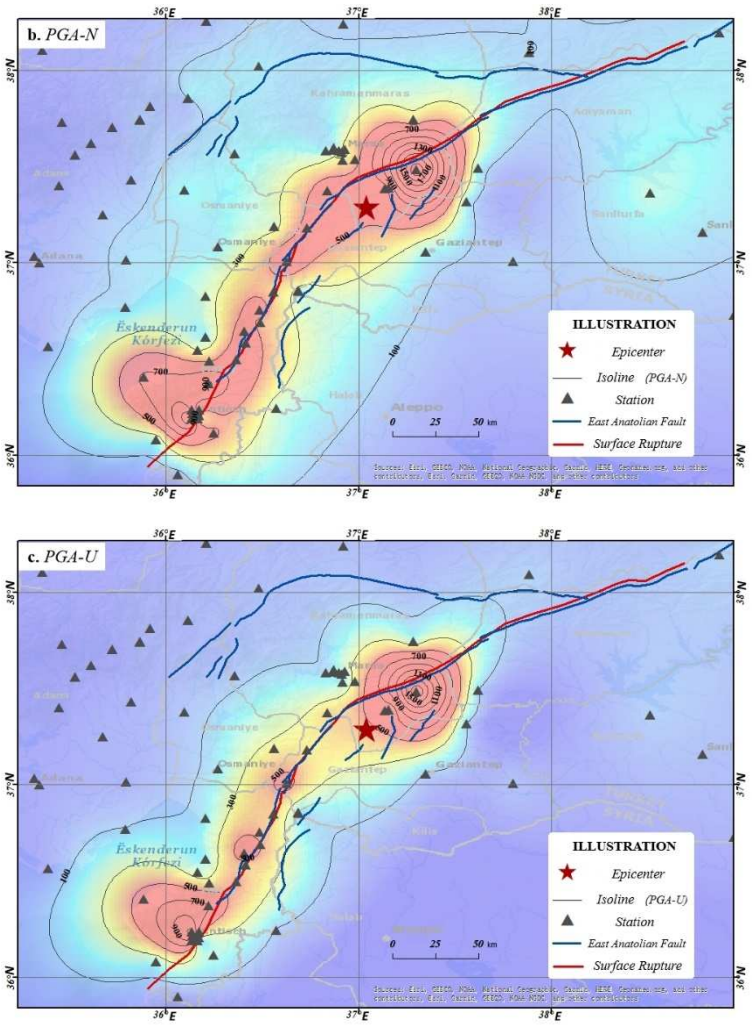

Figure 9. Contour Map of PGA.

4. Discussion

4.1. Discussion on Concentration of Near-Fault Strong Ground Motions

The presence of ample seismic damage data suggests that regions located near fault lines tend to experience the most extensive and severe damage [24]. Research conducted on significant earthquakes, such as the Chi-Chi Earthquake, Chilean Earthquake, Wenchuan Earthquake, Hanshin Earthquake, and New Zealand Earthquake [25,26] have consistently demonstrated that both strong motion observations and numerical simulations indicate a concentration of intense ground motions within a narrow annular region that is centered on the surface projection of the fault [27]. The concentration of strong ground motion is primarily attributed to the geometric attenuation of seismic wave energy radiated from the fault slip source [28]. Analyzing Figure 9, it is evident that the strong ground motions along the fault rupture of this earthquake in Turkey exhibit a clear concentration effect. The distribution of contour lines along the East Anatolian Fault rupture zone exhibits a belt-like pattern, which is consistently observed for peak accelerations in all three directions.

Table 3. Statistics of PGA for Near-Fault (Distance < 30 km) Seismic Records.

Fault Distance (km)		0--5	5--10	10--15	15--20	20--25	25--30
Mean PGA *(cm/s²)*	**Horizontal**	692.49	614.25	314.92	244.64	122.81	135.90
	North-South	674.19	614.40	375.94	250.61	138.02	104.94
	Vertical	561.37	539.45	283.61	172.11	102.38	69.21

Preprints (www.preprints.org) | NOT PEER-REVIEWED | Posted: 5 September 2023 doi:10.20944/preprints202309.0237.v1

The presence of high levels of ground motion in close proximity to active faults highlights the existence of a consistent distribution pattern. The investigation of the correlation between the distribution region of intense ground motion, earthquake magnitude, fault depth, fault type, and the rupture process of the fault is of utmost importance in the field of near-fault ground motion research. Studies by Inoue et al. [27] and Liu et al. [28] have utilized dynamic and kinematic source models to investigate the relationship between strong ground motion distribution and parameters such as fault distance, demonstrating that the intensity of near-fault ground motion decreases notably with increasing fault distance. The statistical analysis in this study focuses on the three-component peak ground acceleration (PGA) data located within a 30 km radius of the fault. The specific details can be found in Table 3. Based on the findings, it can be concluded that the average peak acceleration within a 10 km radius of the fault surpasses 500 cm/s². Similarly, within a 20 km radius, the average peak acceleration exceeds 200 cm/s², while within a 30 km radius, it surpasses 100 cm/s². The study also investigates the relationship between peak acceleration and fault distance, as depicted in Figure 10. Clear trends show that peak acceleration significantly attenuates with increasing fault distance. These statistical findings support conclusions from numerical simulation studies.

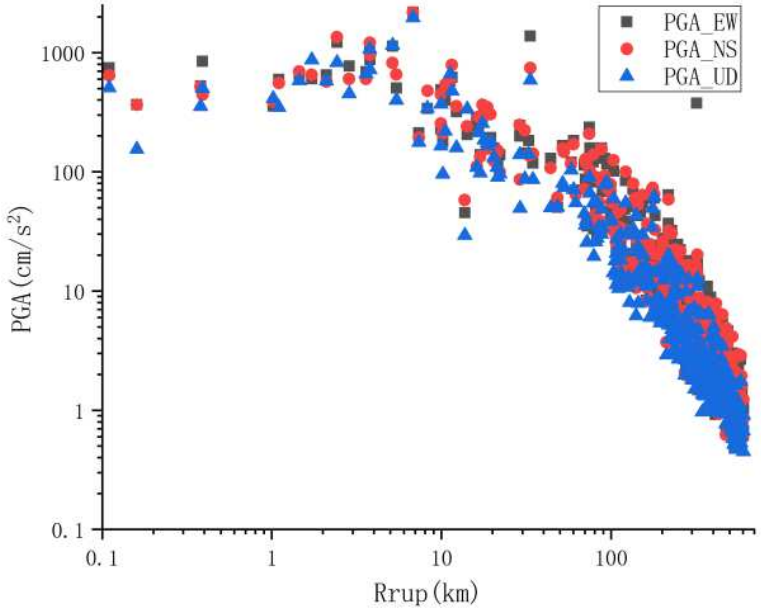

Figure 10. Scatter plot of PGA against fault distance.

4.2. Discussion on Locked Segment Effect

Locked segments are defined as the areas of non-uniform contact between two fault planes. Additionally, they encompass sections of the fault that have not yet experienced rupture or are currently undergoing creeping subduction [29]. Existing research suggests that the movement mode and seismic activity of a fault are influenced by locked segments, and breakthroughs in these locked segments lead to the concentrated release of seismic energy [30]. Prior studies by Qin et al. (2010) [31] and Yang et al. (2017) [32] have validated the locked segment rupture theory through retrospective analysis of typical large earthquakes.

According to the illustration presented in Figure 11, the East Anatolian Main Fault exhibits a division into nine secondary sub-faults. These sub-faults encompass the Amanos FS Segment and the Pazarcik Segment. Every individual sub-fault demonstrates distinct characteristics, including the occurrence of folding and overlapping. Duman et al. (2013) [33], based on active fault mapping and utilizing seismic data from Turkey, confirmed the discontinuous segmented structure of the East Anatolian Fault Zone. Additionally, the authors provided further details regarding the geometric segmentation, intermittent nature of activity, and regional characteristics associated with induced earthquakes.

Preprints (www.preprints.org) | NOT PEER-REVIEWED | Posted: 5 September 2023 doi:10.20944/preprints202309.0237.v1

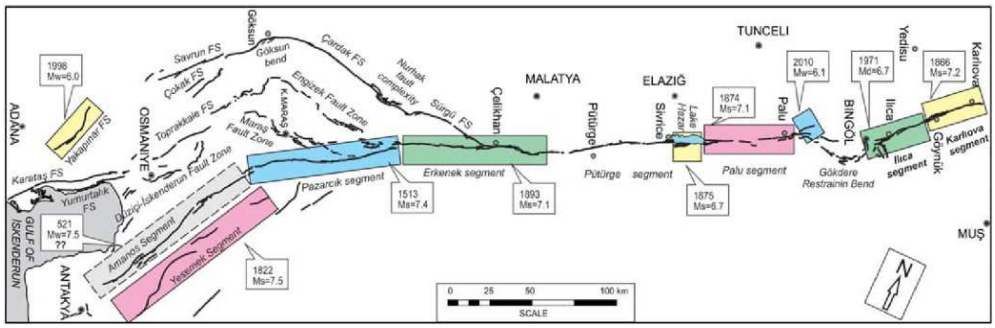

Figure 11. Schematic diagram of surface rupture segments of the East Anatolian Fault and its sub-segments [33]

Upon further examination of Figure 9, it is evident that the distribution of peak ground motion is not continuous. Instead, it is concentrated within specific fault segments, as previously mentioned. This concentration is observed in addition to the band-like concentration along the fault rupture. Figure 12 delineates four distinct regions characterized by significant ground motion peaks, as outlined below:

Region A is located in close proximity to the boundary between the Pazarcik Segment, which is a primary segment of the East Anatolian Main Fault, and the Maras Fault Zone, and this is a secondary sub-fault of the East Anatolian Fault. Centered around station 4614 in Kahramanmaraş city (coordinates N37.485°, E37.298°), the peak acceleration reaches 2039.20 cm/s² at a distance of 31.42 km from the epicenter.

Region B is located at the southwestern end of the Amanos FS Segment, which is a primary segment of the East Anatolian Main Fault. This region serves as the southernmost boundary of the Anatolian Fault. Centered around station 2718 in İslahiye city (coordinates N37.008°, E36.627°), the peak acceleration is 693.81 cm/s² at a distance of 48.30 km from the epicenter.

Region C is situated in close proximity to the bending point of the Amanos FS Segment, more specifically known as the Islahiye releasing bend. Centered around station 3137 in Hatay city (coordinates N36.489°, E36.693°), the peak acceleration is 670.17 cm/s² at a distance of 82.46 km from the epicenter.

Region D is near the left-lateral faulting area of the Amanos FS Segment, known as the Demrek restraining stepover. Centered around station 3129 in Defne city (coordinates N36.191°, E36.134°), the peak acceleration reaches 1351.50 cm/s² at a distance of 146.39 km from the epicenter.

The four regions are situated in close proximity to local overlaps, bends, or terminations of the East Anatolian Fault. These areas frequently exhibit concentrated stress patterns and experience multiple reflections and refractions of seismic waves, which are further influenced by inertia forces. This combination of factors makes these regions prone to experience elevated ground motion [31,34,35]. The concentrated distribution of peak ground motion in these four regions signifies the locked segment effects and suggests higher ground motion intensity and severe seismic damage near these segments.

Preprints (www.preprints.org) | NOT PEER-REVIEWED | Posted: 5 September 2023 doi:10.20944/preprints202309.0237.v1

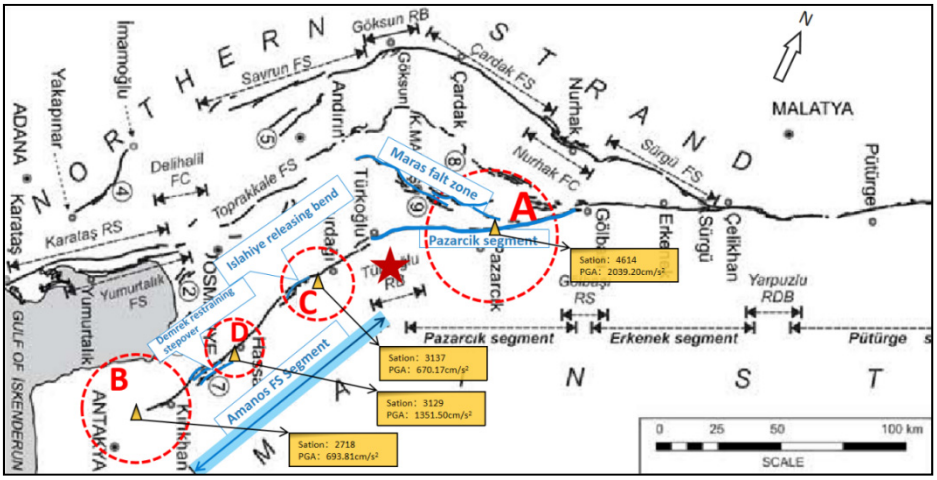

Figure 12. Distribution of high-value PGA near locked fault segments

4.3. Discussion on the Trampoline Effect

In seismic design, the influence of vertical ground motion on structural response sometimes needs to be considered, and this influence is often specified by a certain proportion of horizontal ground motion[34]. In general, the vertical acceleration is about 1/2 to 2/3 of the horizontal one[35]. With the development of strong motion technology, the number of strong motion stations has increased rapidly, and more near-field strong motion records have been obtained, thus people have a deeper and more comprehensive understanding of strong motion records. Especially in recent years, more and more earthquake records with larger vertical peak acceleration have attracted people's attention.

The trampoline effect refers to the phenomenon that when seismic waves reach the ground surface, the surface layer will be compressed and bounced up, just like a trampoline. When the surface layer recovers its elasticity, it will produce an upward reaction force, which will increase the ground acceleration (as shown in Figure 13). This effect was proposed by Aoi S. et al. (2008, Science)[36] to explain the phenomenon that the vertical acceleration is significantly larger than (or even several times larger than) the horizontal acceleration, and that the vertical upward acceleration is significantly larger than the downward acceleration. Aoi S. et al. studied the 3866cm/s^2 vertical acceleration (which is the largest vertical acceleration recorded so far) produced by the Mw6.9 Iwate-Miyagi earthquake on June 14, 2008, and found that the vertical ground acceleration showed a clear asymmetry, with the peak value in the upward direction being about 1.6 times that in the downward direction. This strong motion pattern may promote the seismic evaluation in the near-source area, and have important implications for building design and disaster prevention[36]. Brendon A. et al. (2011)[37] and Meng Lingyuan et al. (2013)[38] observed and verified the trampoline effect in their studies on New Zealand earthquakes, and further analyzed its generation mechanism.

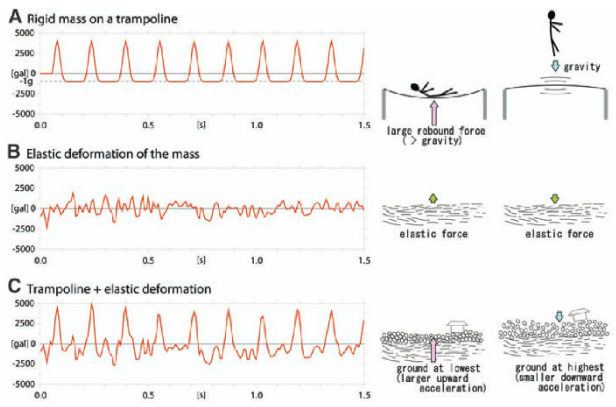

Figure 13. Schematic diagram of the trampoline effect[36]

Preprints (www.preprints.org) | NOT PEER-REVIEWED | Posted: 5 September 2023 doi:10.20944/preprints202309.0237.v1

This paper calculated the ratio of vertical ground motion to horizontal ground motion peak acceleration (V/H) and its relationship with the number of stations, as shown in Figure 14. After analysis, it was found that there were 172 stations with a vertical-to-horizontal acceleration ratio greater than 2/3 in this earthquake motion, accounting for 48% of the total number of records. Through further analysis of typical vertical and horizontal acceleration records, it was found that station 3123 located in Hatay city (coordinates E36.160°, N36.214°, fault distance 1.72km) had a vertical peak acceleration of 867.58cm/s², which was 1.46 times that of the north-south direction (593.94cm/s²); what was more noteworthy was that its vertical upward peak acceleration of 867.58cm/s² was much larger than its downward peak acceleration of 470.46cm/s² (the upward direction was 1.84 times that of the downward direction), as shown in Figure 15, which was a typical manifestation of the trampoline effect in this earthquake.

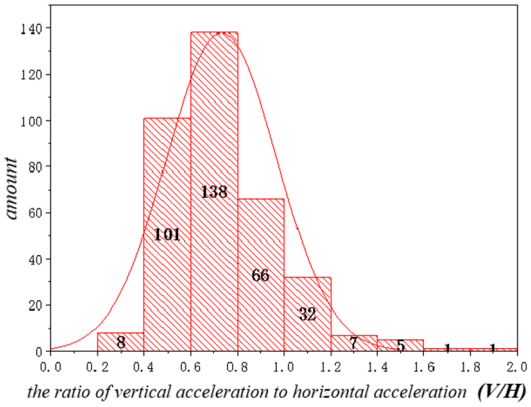

Figure 14. Distribution curve of acceleration V/H number

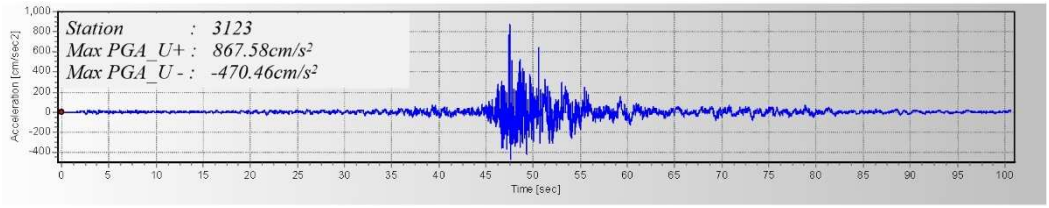

Figure 15. Typical vertical acceleration time history curve showing the trampoline effect

5. Conclusions

Turkey is a seismic hotspot due to its location at the boundary between the Eurasian and Arabian tectonic plates, which is characterised by complex interactions between various tectonic plates and fault systems. The Mw7.8 earthquake, occurred on February 6, 2023, stands as the most devastating earthquake in Turkey since 1900. Using information provided by the Turkish Disaster and Emergency Management Authority (AFAD) and the geometric features of the rupture fault, this study examines the aspects of severe ground motion and their relevance to the fault rupture from a number of different angles. The analysis provides significant contributions regarding the seismic characteristics, strong motion patterns, and subsequent detailed investigations related to the destruction pattern, characteristics, and seismogenic mechanisms of this particular earthquake. The primary findings derived from this study can be summarized as follows:

(1) The seismic event resulted in a substantial amount of strong motion record data, with a total of 397 stations capturing the earthquake's effects. The station 4614 registered the highest peak acceleration ever recorded in Turkey, measuring 2039.20 cm/s² in the north-south direction. A total of 22 stations were located within a 10 km radius of the East Anatolian Fault, which allowed for the collection of valuable records in close proximity to active faults. The acquisition of near-fault seismic records is of great importance in enhancing our understanding of near-field ground motion and providing insights into the size and slip characteristics of seismic faults.

(2) The phenomenon of the concentration effect of strong ground motion in close proximity to active faults is readily observable. The distribution of peak accelerations along the near-fault area shows a band-like pattern, with a noticeable trend of decreasing acceleration as the fault distance increases. The average peak acceleration within a 10 km radius of the fault surpasses 500 cm/s², within a 20 km radius surpasses 200 cm/s², and within a 30 km radius surpasses 100 cm/s².

(3)Locked segment effects influence the distribution of high-value ground motion is influenced by the effects of locked segments. The concentration of strong ground motion is observed in four distinct regions along the East Anatolian Fault Zone. These regions include: the vicinity of the boundary between the Pazarcik segment and the Maras fault zone, the southwestern part of the Amanos FS segment, the area of the Islahiye releasing bend located in the middle of the Amanos FS segment, and the region near the left-lateral faulting area of the Demrek restraining stepover, also situated in the middle of the Amanos FS segment.

(4) The trampoline effect was typically manifested in this earthquake. The vertical-to-horizontal acceleration ratio of 172 stations was greater than 2/3, accounting for 48% of the total number of records. Station 3123 located in Hatay city had a vertical upward peak acceleration of 867.58cm/s², which was much larger than its downward peak acceleration of 470.46cm/s², a typical manifestation of the trampoline effect in this earthquake.

This paper did not consider the influence of permanent ground displacement (residual displacement) in the strong motion data processing, which may exist in some near-source stations, caused by instrument displacement, tilt or site liquefaction and other seismic damage phenomena. Due to the lack of reliable data on permanent displacement, this paper did not consider these residual displacements, which need to be further discussed in detail in future research.

Author Contributions: software, Peng Da; validation, Wenhao Qi; data curation, Qi Li; writing—original draft preparation, Yushi Duan and Wei Wan; writing—review and editing, Yushi Duan and Peng Da; supervision, Jingshan Bo. All authors have read and agreed to the published version of the manuscript.

Funding: This research was funded by NSFC, grant number U1939209 and the Fundamental Research Funds for the Central Universities of Institute of Disaster Prevention, grant number ZY20215121.

Institutional Review Board Statement: Not applicable.

Informed Consent Statement: Not applicable.

Data Availability Statement: The raw data presented in this study are openly available at https://tadas.afad.gov.tr/map. The other data used to support the findings of the study are available from the author upon request. The author's email address is duanyushi2023@163.com.

Acknowledgments: We gratefully acknowledge the Disaster and Emergency Management Authority (AFAD) of Turkey for providing the strong ground motion records of the stations through their official website. We appreciate the professional language services provided by EditSprings (https://www.editsprings.cn).

Conflicts of Interest: The authors declare no conflict of interest.

References

1. Sandıkkaya M A ;Yılmaz M T; Bakır B S, et al. Site classification of Turkish national strong-motion stations[J]. Journal of Seismology, 2010, 14: 543-563.
2. https://link.springer.com/article/10.1007/s10950-009-9176-9 The recently compiled Turkish strong motion database: preliminary investigation for seismological parameters | SpringerLink
3. https://link.springer.com/chapter/10.1007/978-94-007-0152-6_4 Frontiers | Relationship Between Asperities and Velocity Pulse Generation Mechanism
4. Akkar S;Bommer J J. Prediction of elastic displacement response spectra in Europe and the Middle East[J]. Earthquake Engineering & Structural Dynamics, 2007, 36(10): 1275-1301.
5. Beyhan G;Keskinsezer A;Kafadar Ö. Analysis of strong ground motion data from the Van earthquake (Turkey), 2011[J]. Geomechanics and Geophysics for Geo-Energy and Geo-Resources, 2019, 5: 253-270.
6. Akkar S;Bommer J J. Empirical equations for the prediction of PGA, PGV, and spectral accelerations in Europe, the Mediterranean region, and the Middle East[J]. Seismological Research Letters, 2010, 81(2): 195-206.

7. Jackson, J.; McKenzie, D. (1988). The relationship between plate motions and seismic moment tensors, and the rates of active deformation in the Mediterranean and Middle East. Geophysical Journal International, 93(1), 45–73.
8. Jackson; James (1992). Partitioning of strike-slip and convergent motion between Eurasia and Arabia in eastern Turkey and the Caucasus. Journal of Geophysical Research, 97(B9), 12471–. doi:10.1029/92jb00944
9. WESTAWAY, R. O. B.; ARGER, J. A. N. (1996). The Golba i basin, southeastern Turkey: a complex discontinuity in a major strike-slip fault zone. Journal of the Geological Society, 153(5), 729–744. doi:10.1144/gsjgs.153.5.0729
10. Ross S. Stein; Aykut A. Barka; James H. Dieterich (1997). Progressive failure on the North Anatolian fault since 1939 by earthquake stress triggering. , 128(3), 594–604. doi:10.1111/j.1365-246x.1997.tb05321.x
11. Tuncay Taymaz; Haluk Eyido; James Jackson (1991). Source parameters of large earthquakes in the East Anatolian Fault Zone (Turkey). , 106(3), 537–550. doi:10.1111/j.1365-246x.1991.tb06328.x
12. Bulut, Fatih; Bohnhoff, Marco; Eken, Tuna; Janssen, Christoph; Kılıç, Tuğbay; Dresen, Georg (2012). The East Anatolian Fault Zone: Seismotectonic setting and spatiotemporal characteristics of seismicity based on precise earthquake locations. Journal of Geophysical Research, 117(B7), B07304–. doi:10.1029/2011jb008966
13. Tuncay Taymaz; Haluk Eyidoganet, et al. Source parameters of large earthquakes in the East Anatolian Fault Zone (Turkey) [J]. Geophys. J. Int. (1991) 106, 537-550
14. T. C. The Ministry of Culture and Tourism General Directorate of Cultural Heritage and Museums (2023). Depremden Etkilenen İllerimizde Bulunan Müzelerimiz ve Dünya Miras Alanlarımıza İlişkin 9.2.2023 Tarihli Açıklama.
15. Earthquake Damage in Türkiye Estimated to Exceed $34 billion: World Bank Disaster Assessment Report. https://www.worldbank.org/en/news/press-release/2023/02/27/earthquake-damage-in-turkiye-estimated-to-exceed-34-billion-world-bank-disaster-assessment-report
16. Karataş, L.; Ateş, T.; Alptekin, A.; Dal, M.; Yakar, M. (2023). A systematic method for post-earthquake damage assessment: Case study of the Antep Castle, Türkiye. Advanced Engineering Science, 3, 62-71
17. Mavroulis S; Mavrouli M; Vassilakis E, et al. Debris Management in Turkey Provinces Affected by the 6 February 2023 Earthquakes: Challenges during Recovery and Potential Health and Environmental Risks[J]. Applied Sciences, 2023, 13(15): 8823.
18. Preliminary mapping of liquefaction phenomena triggered by the February 6 2023 M7.7 earthquake, Türkiye / Syria, based on remote sensing data Technical Report · February 2023. DOI: 10.5281/zenodo.7668401
19. Dal Zilio L; Ampuero J P. Earthquake doublet in Turkey and Syria[J]. Communications Earth & Environment, 2023, 4(1): 71.
20. Baltzopoulos G; Chioccarelli E; Cito P, et al. Preliminary Engineering Report on Ground Motion Data of the Feb. 2023 Turkey Seismic Sequence[J]. Earthquake reports, 2023.
21. Disaster and Emergency Management Authority. (1973). Turkish National Strong Motion Network [Data set]. Department of Earthquake, Disaster and Emergency Management Authority. https://doi.org/10.7914/SN/TK
22. Moshou A; Konstantaras A; Argyrakis P, et al. Data Management and Processing in Seismology: An Application of Big Data Analysis for the Doublet Earthquake of 2021, 03 March, Elassona, Central Greece[J]. Applied Sciences, 2022, 12(15): 7446.
23. Li Xiaojun. Thoughts on the seismic damage phenomena and engineering seismic problems of recent large earthquakes[J]. International Seismic Dynamics, 2001(08):26-32.
24. Nuti C, Briseghella B; Lavorato D, et al. Effects of Near-Fault Ground Motions on Civil Infrastructure[J]. Applied Sciences, 2023, 13(10): 5929.
25. Chen, K. H.; Furumura, T.; Rubinstein, J.; Rau, R.-J. (2011). Observations of changes in waveform character induced by the 1999 Mw7.6 Chi-Chi earthquake. Geophysical Research Letters, 38(23), n/a–n/a. doi:10.1029/2011gl049841
26. Ulusay R; Tuncay E; Sonmez H, et al. An attenuation relationship based on Turkish strong motion data and iso-acceleration map of Turkey[J]. Engineering Geology, 2004, 74(3-4): 265-291.
27. Inoue T; Miyatake T. 3D simulation of near-field strong ground motion based on dynamic modeling[J]. Bulletin of the Seismological Society of America, 1998, 88(6): 1445-1456.
28. Liu Qifang; Yuan Yifan; Jin Xing; Ding Haiping. Basic characteristics of near-fault ground motion[J]. Earthquake Engineering and Engineering Vibration, 2006,(01):1-10.
29. Xu Qiang; Li Weile. Study on the distribution of large-scale landslides induced by the Wenchuan earthquake[J]. Journal of Engineering Geology, 2010, 18(06):818-826.
30. Huang Runqiu. Large-scale landslides and their occurrence mechanisms in China since the 20th century[J]. Chinese Journal of Rock Mechanics and Engineering, 2007, No.182(03):433-454.

31. Qin Siqing; Xue Lei; Wang Yuanyuan et al. Further verification of the brittle fracture theory of multi-locked segments of seismogenic faults and discussion on related scientific issues[J]. Progress in Geophysics, 2010, 25(03):749-758.
32. YANG Bai-cun; QIN Si-qing; XUE Lei，et al．2017．On the equivalence between the cumulative Benioff strain and the shear strain for the locked patchesalong a seismogenic fault system．Progress in Geophysics ，32(3):1067-1070．
33. Duman T Y; Duman T Y; Emre O. The East Anatolian Fault: geometry, segmentation and jog characteristics[J]. Geological Society, London, Special Publications, 2013, 372(1): 495-529.
34. Hu Yuxian. Seismic Engineering[M]. Beijing: Seismological Press, 1988.
35. Zhou Zhenghua; Zhou Yongnian; Zhao Gang. Statistical analysis of peak acceleration ratio and response spectrum in strong earthquake near-field[J]. Earthquake Engineering and Engineering Vibration, 2002, 22(3): 15-18.
36. Aoi S; Kunugi T; Fujiwara H. Trampoline effect in extreme ground motion[J]. Science, 2008, 322(5902): 727-730.
37. Bradley B A; Cubrinovski M. Near-source strong ground motions observed in the 22 February 2011 Christchurch earthquake[J]. Seismological Research Letters, 2011, 82(6): 853-865.
38. Meng Lingyuan; Shi Baoping; Liu Jie. Comparative analysis of near-field strong ground motion characteristics of the 2010 New Zealand Mw7.0 mainshock and the 2011 Mw6.1 aftershock[J]. Acta Seismologica Sinica, 2013, 35(3): 351-368.